

arXiv:mtl-th/9510001v1 2 Oct 1995

Composition Dependence of the Structure and Electronic Properties of Liquid Ga-Se Alloys Studied by Ab Initio Molecular Dynamics Simulation

J. M. Holender* and M. J. Gillan†

Physics Department, Keele University, Staffordshire ST5 5BG, U.K.

Ab initio molecular dynamics simulation is used to study the structure and electronic properties of the liquid Ga-Se system at the three compositions Ga_2Se , GaSe and Ga_2Se_3 , and of the GaSe and Ga_2Se_3 crystals. The calculated equilibrium structure of GaSe crystal agrees well with available experimental data. The neutron-weighted liquid structure factors calculated from the simulations are in reasonable agreement with recent neutron diffraction measurements. Simulation results for the partial radial distribution functions show that the liquid structure is closely related to that of the crystals. A close similarity between solid and liquid is also found for the electronic density of states and charge density. The calculated electronic conductivity decreases strongly with increasing Se content, in accord with experimental measurements.

61.20.Ja, 61.25.Mv, 71.25.Lf, 72.80.Ph

I. INTRODUCTION

The study of liquid semiconductor alloys goes back many years, and has been a splendid source of insights into the relationships between atomic ordering, chemical bonding and electrical properties in condensed matter¹. In some well studied systems like Cs-Au² and Mg-Bi³, where the elements have rather different electronegativities, the electrical conductivity passes from highly metallic values to insulating values, as a gap at the Fermi level opens up in the density of states and the bonding changes from metallic to ionic at the stoichiometric composition. In cases where one element is a metal and the other a semiconductor in the liquid state, the chemical bonding can be continuously tuned from metallic to covalent as the composition is varied. The Ga-Se system studied in this paper is an example of the latter kind.

We have used *ab initio* molecular dynamics simulation⁴ (AIMD) to study the liquid Ga-Se alloy at the three compositions Ga_2Se , GaSe and Ga_2Se_3 . The simulations have been used to study the liquid structure, the electronic density of states and the spatial distribution of electrons as a function of composition. We shall show that the relationship between the properties of the solid and the liquid is very instructive, and we have used the same methods to study the two stoichiometric solids GaSe and Ga_2Se_3 .

The liquid Ga-Se system has been rather little studied experimentally, and we chose to work on it mainly because we were aware of plans to perform neutron diffraction measurements on the system⁵. These measurements, as well as studies of the electrical conductivity, were completed while the work was in progress, and we shall present comparisons with both sets of results. The system is also expected to show quite a close resemblance to the liquid alloys In-Se (the electronic properties have been studied by Okada and Ohno⁶), Ga-Te (structure measurements have been done by Takeda *et al.*⁷ and Hoyer *et al.*⁸ and electronic properties by Valiant and Faber⁹) and In-Te (structure measurements have been made by Hoyer *et al.*¹⁰, conductivity and thermopower by Popp *et al.*¹¹).

It is useful to consider what structural and electronic changes would be expected as the composition of ℓ -Ga-Se is varied. Liquid Ga is a typical liquid metal, with a coordination number of $\sim 9^{12}$, while ℓ -Se has a covalently bonded chain-like structure with a coordination number of 2 (Ref. 13). It is clear then that there must be radical changes of structure across the composition range. However, the electronegativity difference between Ga and Se is fairly small, so that strongly ionic bonding is not expected. This is confirmed by the structure of the crystals. In the rather unusual layer structure of GaSe ¹⁴, the Ga atoms are tetrahedrally bonded to Se and to each other, and the Se atoms have threefold coordination to Ga. The Ga_2Se_3 crystal¹⁵ shows tetrahedral coordination of both elements. In the middle concentration range of the liquid, we might therefore expect a covalently bonded low-coordinated structure dominated by Ga-Ga and Ga-Se bonds. This expectation is fully confirmed by our simulations.

The AIMD technique is ideally suited to this type of problem. The basic principle is that the total energy of the system and the forces on the atoms for any atomic arrangement are calculated by solving Schrödinger's equation for the valence electrons to find the self-consistent ground state. By simulating the system in thermal equilibrium, we therefore generate the liquid structure, the chemical bonding and the electronic structure in a completely unified way, and without any prior assumptions or adjustable parameters. In the past few years, AIMD has become a widely used

technique for studying liquid metals and semiconductors^{16,17}. The work reported here is closely related to our recent simulations of ℓ -Ga¹⁸ and ℓ -Ag-Se¹⁹.

The paper is organized as follows. In the following section, we summarize the AIMD techniques we use. Sec. 3 presents our calculations on the equilibrium structure and electronic structure of the crystals. Our AIMD simulations on the liquid alloys are then reported in Sec. 4. The significance of the results and comparisons with related liquid alloys are discussed in Sec. 5.

II. TECHNIQUES

The first-principles simulation methods used here are the same as those used in our work on ℓ -Ga¹⁸, and we give only a brief summary of the main points. Only valence electrons are treated explicitly, and the core states are assumed to be identical to those in the free atoms. For the Ga-Se system, all states up to and including the $3d$ states in both species are treated as part of the core. The interactions between valence electrons and the cores are represented by norm-conserving nonlocal pseudopotentials, which are constructed *ab initio* via calculations on the free atoms (see below). The calculations are performed in periodic boundary conditions, with the electronic orbitals expanded in plane waves, all plane waves being included whose kinetic energy is less than a chosen cutoff E_{cut} . The exchange-correlation energy is represented by the local density approximation (LDA), the form used here being that due to Ceperley and Alder²⁰. In the dynamical simulations, the ions follow classical trajectories determined by the Hellmann-Feynman forces obtained from the first-principles calculations, while the electronic sub-system remains in the ground state at every instant (the Born-Oppenheimer principle).

The problems of performing accurate first-principles simulations on metallic systems have been extensively discussed in the literature^{18,21-23}. We use here the Fermi-smearing technique with orbital occupation numbers treated as dynamical variables. The smearing is handled with the quasi-Gaussian smearing function introduced in our ℓ -Ga work¹⁸. Minimization of the (free) energy to obtain the self-consistent ground state for each ionic configuration is performed by the preconditioned conjugate gradients method. The calculations were performed with the all-bands version of the CASTEP code²⁴ running on the Fujitsu VPX 240 at Manchester.

The norm-conserving pseudopotential for Ga is identical to the one used in our ℓ -Ga work. For Se, we generated a pseudopotential using the standard Kerker²⁵ method. The s and p components of the pseudopotential were generated using the atomic configuration $4s^24p^4$, and the d component using the configuration $4s^24p^{2.75}4d^{0.25}$. The core radii were taken to be 2.0, 2.0 and 2.3 a.u. for s , p and d components respectively. The pseudopotentials were represented in the Kleinman-Bylander form²⁶, with the p -wave treated as local for both Ga and Se, and the non-local parts of the pseudopotentials treated in real space²⁷.

The electronic densities of states (DOS) for the solids were calculated using the standard tetrahedron method²⁸. For the liquids we used two approaches. The first method was to use Γ -point sampling only and to average over all ionic configurations, and the second was to use many k -points for a few chosen configurations. Both methods gave essentially the same DOS.

III. CRYSTALLINE PHASES

The β -GaSe crystal has the layered structure shown in Fig. 1, with every layer consisting of four planes of atoms. Each of these planes contains one type of atom, the ordering of the planes being Se-Ga-Ga-Se. The symmetry of the crystal is hexagonal, with the hexagonal axis perpendicular to the layers, and the atoms in each plane are arranged in a regular close-packed hexagonal lattice. The interatomic bonding is strong within each layer, but weak between the layers, and this means that there are different ways of stacking the layers which have almost the same energy. Four polytypes differing in the stacking are experimentally known¹⁴, and the observed form depends on the preparation method. There has been controversy about which polytype is most stable.

Our aims in studying the crystal are to test our pseudopotentials and to obtain an understanding of the electronic structure, so that our main concern is with the strong intra-layer bonding. For this purpose, it does not matter which polytype we examine, and we have chosen to work with the β -phase, for which rather precise diffraction data are available²⁹. Because of the relation between adjacent layers in this polytype, the primitive cell contains a total of eight atoms. The crystal structure is characterized by the two lattice parameters a and c and the two internal parameters u and v . The u and v parameters specify the positions of the Ga and Se planes respectively along the c -axis. (For a detailed definition, see Wyckoff³⁰; the z -coordinates for Ga and Se used in the paper of Benazeth *et al.*²⁹ correspond exactly to these u and v parameters.)

The calculations on β -GaSe were performed using a plane-wave cutoff of 250 eV. This cutoff was chosen on the basis of systematic tests on the convergence of the total energy as a function of cutoff, which showed that the residual error is roughly 1 meV per 8-atom cell. Brillouin-zone sampling was performed using 18 Chadi-Cohen points³¹ in the full zone. Again, tests done with different k -point sets indicate that the residual error is no more than a few meV per cell.

We have performed a full structural relaxation of the crystal, which gives the following equilibrium parameters (experimental values in parentheses): $a = 3.64 \text{ \AA}$ (3.750 \AA), $c = 15.76 \text{ \AA}$ (15.995 \AA), $u = 0.174$ (0.1736) and $v = 0.602$ (0.6015). The reasonably close agreement with experiment fully confirms the adequacy of our pseudopotentials. A slight underestimation of lattice parameters is commonly found in DFT calculations, and we note that the calculated lattice parameter in our earlier work on crystalline Ga was also too low by $\sim 3\%$. During the relaxation process, we have noted the expected strong anisotropy in the energetics of the crystal³², with changes of the c -parameter causing much smaller energy changes than those of the a -parameter.

The electronic DOS calculated for the equilibrium structure is shown in Fig. 2 (upper panel). The calculations indicate that the material is a semiconductor, with a band gap of 1.35 eV (experimentally about 2 eV³³). The electronic structure of β -GaSe was studied many years ago by Schlüter³⁴ using an empirical model pseudopotential, and we find that his band structure is in semi-quantitative agreement with our results. So far as we know, ours are the first *ab initio* calculations on the electronic structure of GaSe.

The valence part of the DOS consists of an isolated peak at -14 eV (bands 1-4), a double peak at -8 eV (bands 5-6 and 7-8), and a broader distribution extending from -6 eV up to the valence band maximum (VBM) (bands 9-18). A clearer understanding of these features can be obtained by studying the partial electron densities associated with chosen energy ranges. These densities (Fig. 3) show that the peak at -14 eV arises from Se(4s) states, while the double peak arises from bonding and anti-bonding states associated with Ga-Ga pairs, but with some weight on neighboring Se atoms. These states can be regarded as made of Ga(4s) states, with a strong admixture of other states. The broad peak in the DOS between -6 eV and the VBM appears to be mainly responsible for bonding in the material, and consists of Ga(4p) and Se(4p) states. This general analysis is consistent with what was found by Schlüter³⁴. It is interesting to note that there have been recent first-principles calculations on the closely related material InSe³⁵, and the DOS calculated for that system shows all the same qualitative features as ours.

We have also performed calculations on the Ga_2Se_3 crystal, though here the experimental situation is rather unsatisfactory. Again, there are a number of closely related structures, all of which appear to be based on a defective zinc-blende structure, in which one third of the cation sites are vacant. One of these (γ - Ga_2Se_3 , which is the high temperature phase) has full cubic symmetry, and the distribution of vacancies appears to be random¹⁵.

Our Ga_2Se_3 calculations were performed on a periodic system having an 80-atom cell ($\text{Ga}_{32}\text{Se}_{48}$) consisting of twelve adjacent zinc-blende cubes, with sixteen, randomly chosen, vacant cation sites per cell. For this system we have calculated the electronic density of states (without relaxing the system) and the valence-charge density. The calculations have been performed with the same plane-wave cutoff as for β -GaSe.

The electronic DOS is shown in Fig. 2 (lower panel). Again, we are dealing with a semiconductor, the gap in this case being about 0.6 eV. The valence DOS consists of the Se(4s) peak at about -14 eV and a broader distribution from -10 eV up to the energy gap. The peaks in the DOS are not so well visible as in the case of β -GaSe because of the randomness of γ - Ga_2Se_3 .

IV. LIQUID ALLOYS

A. Structure and dynamics

We have performed AIMD simulations of the liquid Ga-Se system for the three compositions Ga_2Se , GaSe and Ga_2Se_3 at the temperature 1300 K. All the simulations were done on a repeating system of 60 atoms using Γ -point sampling, with a plane-wave cut-off of 150 eV. This cut-off is less than the one used for calculations on the solids, but is adequate for simulations of the liquids. The time step was taken to be 3 fs, and the Fermi smearing was 0.2 eV. The density of these liquid mixtures is not experimentally known, and the densities we use are obtained from experimental values for ℓ -Ga and ℓ -Se. Data for the density of ℓ -Ga are available up to ~ 1000 K, and the value at 1300 K can be estimated by a small extrapolation. The case of ℓ -Se is more tricky, since the boiling point under atmospheric pressure is only 958 K. We have estimated the (hypothetical) density at 1300 K by linear extrapolation of experimental data between 490 and 958 K. Finally, the densities of the liquid mixtures at 1300 K are obtained by linear interpolation between the estimated values for ℓ -Ga and ℓ -Se at this temperature. Some time after the work was started, a cross-check became possible against recent neutron diffraction data on ℓ -Ga-Se at the same three compositions⁵, and this showed that our estimated densities were correct to within better than 5 % in all cases. It

is worth mentioning that linear interpolation between *c*-Ga and *c*-Se predicts the densities of solid GaSe and Ga₂Se₃ very accurately.

We initiated the simulations by starting from a typical configuration of atoms taken from our previous *l*-Ga simulations¹⁸, and replacing some of the Ga atoms by Se atoms. At each composition, our simulated system was equilibrated for 1 ps, and then a production run of 4 ps was generated. The temperature and liquid structure were monitored throughout the simulations, and the stability of these quantities indicated that the 1 ps equilibration period was adequate.

The structure of the simulated liquid can be compared directly with that of the real system through the static structure factors $S_{\alpha\beta}(k)$. These quantities, which give a measure of the intensity of density fluctuations as a function of wavevector k , are defined by:

$$S_{\alpha\beta}(k) = \langle \hat{\rho}_\alpha(\mathbf{k}) \hat{\rho}_\beta^*(\mathbf{k}) \rangle . \quad (1)$$

Here the dynamical variable $\hat{\rho}_\alpha(\mathbf{k})$ representing the Fourier component of the atomic density of atoms type α at wavevector \mathbf{k} is given by:

$$\hat{\rho}(\mathbf{k}) = N_\alpha^{-1/2} \sum_{i=1}^{N_\alpha} \exp(i\mathbf{k} \cdot \mathbf{r}_i) , \quad (2)$$

where \mathbf{r}_i is the position of atom i and N_α is the number of atoms of type α in the system. The angular brackets in Eq. (1) denote the thermal average, which in practice is evaluated as the time average over the duration of the simulation. The structure factors were calculated for vectors \mathbf{k} compatible with the periodic boundary conditions. In practical calculations of $S_{\alpha\beta}(k)$, we also average over \mathbf{k} vectors having the same magnitude. The neutron weighted structure factor $S_n(k)$ measured in a neutron diffraction experiment is given by:

$$S_n(k) = \frac{\sum_{\alpha\beta} \sqrt{c_\alpha c_\beta} b_\alpha b_\beta S_{\alpha\beta}(k)}{\sum_\alpha c_\alpha b_\alpha^2} , \quad (3)$$

where c_α and b_α are the concentration and the neutron scattering length of species α respectively. In the present work, we took the scattering lengths for Ga and Se to be $b_{\text{Ga}}=7.288$ fm and $b_{\text{Se}}=7.97$ fm (Ref. 5). We shall also need to refer to the total structure factor $S(k)$, which is defined by:

$$S(k) = \sum_{\alpha\beta} \sqrt{c_\alpha c_\beta} S_{\alpha\beta}(k) . \quad (4)$$

In fact, $S(k)$ is virtually identical to $S_n(k)$ for the present systems, since b_{Ga} and b_{Se} are almost the same.

The neutron-weighted liquid structure factors $S_n(k)$ calculated for the three compositions are compared with the recent neutron diffraction data⁵ in Fig. 4. The agreement is good for wavevectors above ~ 3 Å⁻¹, and is reasonably satisfactory below that. Since the main discrepancies are at low k , it is possible that the rather small size of our simulated system may be influencing the results; limitations of computer power prevent us from going to larger systems at present. The main changes in the experimental $S_n(k)$ with increasing Se content are the appearance of a small peak at ~ 1 Å⁻¹, a shift and enhancement of the peak at ~ 2 Å⁻¹ and an increase in amplitude and shift in phase of the oscillations beyond ~ 3 Å⁻¹. All these effects are correctly reproduced in the simulations.

The origin of the features in $S_n(k)$ can be understood by examining the partial structure factors $S_{\alpha\beta}(k)$ shown in Fig. 5. These results make it clear that the main peak in $S_n(k)$ at ~ 3 Å⁻¹ arises from a superposition of almost coincident peaks in all three $S_{\alpha\beta}(k)$. The peak at ~ 2 Å⁻¹ comes mainly from a peak in $S_{\text{Se}-\text{Se}}(k)$, which is partially cancelled by a trough in $S_{\text{Ga}-\text{Se}}(k)$; both of these features shift to lower k as the Se content is increased. The appearance of the small peak at ~ 1 Å⁻¹ is due mainly to a growth of Ga-Se correlations with increasing Se content.

The real-space structure of the liquid can be understood through the partial radial distribution functions (RDFs) $g_{\alpha\beta}(r)$ (Fig. 6), and the coordination numbers of their first peaks (table I). One can notice very strong similarities between the structures of solids and the corresponding liquids. Not only are the interatomic distances very similar but also the coordination numbers are very close.

It is useful to relate the forms of the RDFs to the corresponding crystal structures. The main peak in $g_{\text{Ga}-\text{Se}}$ arises from directly bonded Ga-Se pairs, and its distance is close to the corresponding bond length in the crystals. The main peak in $g_{\text{Se}-\text{Se}}$ comes from pairs of Se atoms bonded to the same Ga atom, and its distance remains unchanged for the same reason that the Se-Se distance is almost the same in the GaSe and Ga₂Se₃ crystals. We note, however, the formation of a small peak in $g_{\text{Se}-\text{Se}}$ at ~ 2.4 Å at the Ga₂Se₃ composition, which is due to Se atoms directly bonded to each other; this is confirmed by the fact that 2.4 Å is almost exactly the bond length in crystalline³⁰ and liquid

Se^{13} . At low Se content, $g_{\text{Ga-Ga}}$ consists mainly of a peak at $\sim 2.6 \text{ \AA}$, whose height decreases strongly on going to Ga_2Se_3 , with the growth of a second peak at $\sim 3.8 \text{ \AA}$. This is related to the presence of Ga-Ga bonds in crystalline GaSe and their absence in Ga_2Se_3 .

We have studied the diffusion behavior of Ga and Se by calculating the time-dependent mean square displacements for the two species. These show the usual liquid-like behavior, with a rapid transition to a linear dependence on time after about 0.1 ps. The self-diffusion coefficients D_{Ga} and D_{Se} are obtained in the usual way from the slope, and the calculated values are shown in Table II. The results show that both diffusion coefficients decrease rather strongly with increasing Se content, presumably because of the formation of a fairly stable covalently bonded network. Interestingly, though, recent AIMD simulations that we have made on pure $\ell\text{-Se}^{36}$ show that its diffusion coefficient at 1375 K has a high value of $1.5 \times 10^{-4} \text{ cm}^2\text{s}^{-1}$. We conjecture that D_{Se} has a minimum at the composition Ga_2Se_3 and increases rapidly thereafter.

B. Electronic properties

The total electronic densities of states (DOS) of the GaSe and Ga_2Se_3 liquids are compared with our results for the corresponding crystals in Fig. 7. The comparison shows the very close resemblance of the solid and liquid phases, which might be expected from the similarity of their short-range order. In both cases, the liquid-state DOS is simply a rather broadened version of the crystal DOS but shifted to higher energies. The main difference for GaSe is the replacement of the band gap by a minimum in the DOS. The variation of electronic structure with composition is illustrated in Fig. 8, where we include the DOS for $\ell\text{-Ga}$ at 982 K taken from our previous work¹⁸. The $\ell\text{-Ga}$ system is highly metallic, and has a free-electron-like DOS. The change on going to GaSe is very marked, with the appearance of the feature due to $\text{Se}(4s)$ states and the formation of the broad two-component distribution consisting of hybridized $\text{Ga}(4s/p)\text{-Se}(4p)$ states characteristic also of GaSe and Ga_2Se_3 . The DOS at the Fermi level shows a monotonic decrease with increasing Se content, reaching a zero value at the Ga_2Se_3 composition.

The close resemblance between the electronic structure of the solid and liquid is confirmed by a study of the electron density distribution. A useful way to do this in the liquid is to examine the density on a plane passing through two neighboring Ga atoms and a Se atom neighboring one of these Ga atoms. We show in Fig. 9 the energy resolved partial densities for a typical configuration in $\ell\text{-GaSe}$, which can be directly compared with the corresponding results for the crystal (Fig. 3). All the characteristic features found in the solid – the $\text{Se}(4s)$ states (bands 1-30), the bonding and anti-bonding states on the Ga pair (bands 31-45 and 46-60), and the Ga-Se and Ga-Ga bonding states associated with the upper part of the valence band (bands 61-135) – are clearly visible in the liquid. We find a similar close resemblance for solid and liquid Ga_2Se_3 , as illustrated in Fig. 10.

The relation between the electron density distribution in the solid and liquid can be pursued to a more quantitative level. To do this, we have chosen particular Ga-Ga and Ga-Se pairs in liquids of different compositions and in the solids, and plotted the electronic density along the bonds. Since the distances between neighbors vary in the liquid, we reduce lengths to a common scale by dividing by the interatomic distance. Some typical comparisons are shown in Fig. 11. The agreement between the solid-state and liquid-state curves, even for different compositions, is remarkable, and indicates that there is almost no change in the short-range electronic structure between the different phases.

We have calculated the electronic d.c. conductivity of the three liquid phases using the Kubo-Greenwood approximation³⁷. The technique used is the one described in several previous papers^{16,18}. The calculations were done by averaging over the full duration of each simulation, and used Γ -point sampling, which is expected to be adequate for present purposes. Fermi-Dirac thermal occupation numbers were included in the calculations. The results are compared with the very recent experimental measurements of Lague and Barnes⁵ in Fig. 12. In this graph we also include results for pure Ga¹⁸. Given the approximations involved, the agreement is as good as can be expected. The dramatic decrease of conductivity is, of course, associated with the reduction of DOS at the Fermi level already described.

V. DISCUSSION AND CONCLUSIONS

The good agreement between the calculated equilibrium structure of the GaSe crystal with available data, as well as the satisfactory comparisons of the liquid structure factors with recent diffraction data, give confidence in the realism of our AIMD simulations. One of the main findings from these simulations is the very close relation between the properties of the solids and the liquids. The positions of the peaks in the liquid RDFs for GaSe and Ga_2Se_3 are close to the interatomic distances in the crystals, and the coordination numbers are also similar. As suggested in the Introduction, the bonding in the liquids appears to be a mixture of metallic and covalent, with the structure

dominated by Ga-Ga and Ga-Se bonding in the composition range we have examined. These findings about the similarity of solid and liquid and the nature of the bonding are in line with indications from early diffraction work on the related Ga-Te and In-Te liquids⁷.

Clearly at some point in the composition range, direct bonding between Se atoms must become important, since the structure of pure ℓ -Se is entirely determined by this bonding. According to our simulations, this direct bonding is insignificant in the range up Ga_2Se_3 . However, there is clear evidence in the $g_{\text{Se}-\text{Se}}$ RDF for the beginning of this effect at the Ga_2Se_3 composition. It is interesting here to compare with our recent AIMD simulations on the ℓ -Ag-Se system¹⁹, where we found that direct Se-Se bonding begins at the Ag_2Se composition, and rapidly becomes a dominant effect for higher Se contents. This strongly suggests that the point at which Se-Se bonding begins is determined by the maximum valency of the other component. In this context, *ab initio* simulations or diffraction measurements on systems such as Cu-Se and Cd-Se would be extremely interesting.

The strong similarity of solid and liquid is also very clear from our results for the electronic DOS, where we have shown that for both GaSe and Ga_2Se_3 the liquid DOS is essentially a broadened version of the solid DOS, except for the disappearance of the band gap in the case of GaSe . Interestingly, the band gap does not disappear for $\ell\text{-Ga}_2\text{Se}_3$. This behavior of the DOS is closely related to the composition dependence of the electrical conductivity, which, according to our rather limited results, decreases rapidly and monotonically as one passes from $\ell\text{-Ga}$ to $\ell\text{-Ga}_2\text{Se}_3$, as is also found experimentally.

ACKNOWLEDGMENTS

The work of JMH is supported by EPSRC grant GR/H67935. The computations were performed on the Fujitsu VPX 240 at Manchester Computer Centre under EPSRC grant GR/J69974. Analysis of the results made use of distributed hardware provided by EPSRC grant GR/36266. We gratefully acknowledge useful discussions with J.E. Enderby, A.C. Barnes, S.B. Lague and F. Kirchhoff.

* Electronic address: j.m.holender@keele.ac.uk

† Electronic address pha71@keele.ac.uk

¹ J. E. Enderby and A. C. Barnes, *Rep. Prog. Phys.* **53**, 85 (1990).

² R. W. Schmutzler, H. Hoshino, R. Fisher, and F. Hensel, *Ber. Bunsenges. Phys. Chem.* **80**, 107 (1976).

³ J. E. Enderby and E. W. Collings, *J. Non-Cryst. Solids* **4**, 161 (1970).

⁴ R. Car and M. Parrinello, *Phys. Rev. Lett.* **55**, 2471 (1985).

⁵ S. B. Lague, A. C. Barnes, A. D. Archer, and W. S. Howells, *J. Non-Cryst. Solids*, at press.

⁶ T. Okada and S. Ohno, *J. Non-Cryst. Solids* **156-158**, 748 (1993).

⁷ S. Takeda, S. Tamaki, and Y. Waseda, *J. Phys. Soc. Japan* **52**, 2062 (1983).

⁸ W. Hoyer, A. Müller, W. Matz, and M. Wobst, *phys. stat. sol. (a)* **84**, 11 (1984).

⁹ J. C. Valiant and T. E. Faber, *Phil. Mag.* **29**, 571 (1974).

¹⁰ W. Hoyer, A. Müller, E. Thomas, and M. Wobst, *phys. stat. sol. (a)* **72**, 585 (1982).

¹¹ K. Popp, H. U. Tschirner, and M. Wobst, *Phil. Mag.*, **30**, 685 (1974).

¹² M. C. Bellissent-Funel, P. Chieux, D. Levesque and J. J. Weis, *Phys. Rev. B* **39**, 6310 (1989).

¹³ M. Inui, K. Tamura, M. Yao, H. Endo, S. Hosogawa, H. Hoshino, *J. Non-cryst. Solids* **117 & 118**, 112 (1990).

¹⁴ A. Kuhn, A. Chevy, and R. Chevalier, *phys. stat. sol. (a)* **31**, 469 (1975).

¹⁵ J. C. Mikkelsen, *J. Solid State Chem.* **40**, 312 (1981).

¹⁶ I. Štich, R. Car and M. Parrinello, *Phys. Rev. Lett.* **63**, 2240 (1989).

¹⁷ Q. M. Zhang, G. Chiarotti, A. Selloni, R. Car and M. Parrinello, *Phys. Rev. B* **42**, 5071 (1990); G. Galli and M. Parrinello, *J. Chem. Phys.* **95**, 7504 (1991); X. G. Gong, G. L. Chiarotti, M. Parrinello and E. Tosatti, *Europhys. Lett.* **21**, 469 (1993); G. Kresse and J. Hafner, *Phys. Rev. B* **48**, 13115 (1994). G. A. de Wijs, G. Pastore, A. Selloni and W. van der Lugt, *Europhys. Lett.* **27**, 667 (1994); M. Schöne, R. Kaschner and G. Seifert, *J. Phys.: Condens. Matter* **7**, L19 (1995).

¹⁸ J. M. Holender, M. J. Gillan, M. C. Payne, and A. D. Simpson, *Phys. Rev. B* **52**, 967 (1995).

¹⁹ F. Kirchhoff, J. M. Holender, and M. J. Gillan, *Phys. Rev. Lett.* submitted.

²⁰ D. M. Ceperley and B. Alder, *Phys. Rev. Lett.* **45**, 566 (1980); J. Perdew and A. Zunger, *Phys. Rev. B* **23**, 5048 (1981).

²¹ M. J. Gillan, *J. Phys.: Condens. Matter* **1**, 689 (1989).

²² M. P. Grumbach, D. Hohl, R. M. Martin and R. Car, *J. Phys.: Condens. Matter* **6**, 1999 (1994).

²³ G. Kresse and J. Hafner, *Phys. Rev. B* **49**, 14251 (1994).

²⁴ M. C. Payne, M. P. Teter, D. C. Allan, T. A. Arias and J. D. Joannopoulos, Rev. Mod. Phys. **64**, 1045 (1992).
²⁵ G. P. Kerker, J. Phys. C **13**, L189 (1980).
²⁶ L. Kleinman and D. M. Bylander, Phys. Rev. Lett. **48**, 1425 (1982).
²⁷ R. D. King-Smith, M. C. Payne and J. S. Lin, Phys. Rev. B **44**, 13063 (1991).
²⁸ O. Jepsen and O. K. Andersen, Solid State Commun. **9**, 1763 (1971); G. Lehmann and M. Taut, phys. stat. sol. **54**, 469 (1972).
²⁹ P. S. Benazeth, N.-H. Dung, M. Guittard, and P. Laruelle, Acta Cryst. C **44** 234 (1988).
³⁰ R. W. G. Wyckoff, *Crystal Structures*, 2nd edition, vol. 1 (Interscience, New York, 1964).
³¹ D. J. Chadi and M. L. Cohen, Phys. Rev. B **8**, 5747 (1973).
³² G. I. Abutalybov, S. Z. Dzhafarova, and N. A. Ragimova, Phys. Rev. B **51**, 17479 (1995).
³³ J. V. McCann and R. B. Murray, J. Phys. C **10**, 1211 (1977).
³⁴ M. Schlüter, Nuovo Cimento **13B**, 313 (1973).
³⁵ P. Gomes da Costa, R. G. Dandrea, R. F. Wallis, and M. Balkanski, Phys. Rev. B **48**, 14135 (1993).
³⁶ F. Kirchhoff, M. J. Gillan, and J. M. Holender, J. Non-Cryst. Solids, at press.
³⁷ N.F. Mott and E. A. Davies, *Electronic Processes in Non-crystalline Materials*, Clarendon, Oxford 1979.

FIG. 1. Structure of the β -GaSe crystal. Dark and light spheres represent Ga and Se respectively.

FIG. 2. Calculated electronic DOS for β -GaSe (upper panel) and γ -Ga₂Se₃ (lower panel). For presentation purposes, the calculated DOS are convoluted with a Gaussian of width 0.1 eV. The horizontal scale represents the difference of the energy E and the Fermi energy E_F .

FIG. 3. The band-resolved and total charge densities for the β -GaSe crystal (units: 10^{-2} Å⁻³). Ga and Se sites are marked by filled circles and squares respectively. Lengths are marked in Å units. The first four panels show bands resolved charge densities corresponding to features in the DOS (for meaning of bands see text). The last panel shows the total charge density.

FIG. 4. Simulated (solid line) and experimental (circles) neutron-weighted structure factors of liquid Ga-Se at three compositions. The vertical scale refers to the GaSe results, with Ga₂Se and Ga₂Se₃ results shifted respectively up and down by one unit.

FIG. 5. Faber-Ziman partial structure factors $S_{\alpha\beta}(k)$ and total structure factor (see text) obtained from simulations of liquid Ga-Se at three compositions.

FIG. 6. Partial radial distribution functions $g_{\alpha\beta}(r)$ obtained from simulations of liquid Ga-Se at three concentrations. Solid and dashed vertical lines indicate interatomic distances in the β -GaSe and γ -Ga₂Se₃ crystals respectively.

FIG. 7. Comparison of the electronic DOS for solid (—) and liquid (---) GaSe and Ga₂Se₃.

FIG. 8. Comparison of the electronic DOS calculated for ℓ -Ga and ℓ -Ga-Se at three compositions.

FIG. 9. Band-resolved and total electron densities for ℓ -GaSe (units: 10^{-2} Å⁻³). Ga and Se sites are marked by filled circles and squares respectively. Lengths are marked in Å units. The first four panels show bands resolved charge densities corresponding to features in the DOS (for meaning of bands see text). The last panel shows the total charge density.

FIG. 10. Total electron density for solid (left panel) and liquid (right panel) Ga₂Se₃ (units: 10^{-2} Å⁻³). Lengths are marked in Å units.

FIG. 11. Electron density (units: 10^{-2} Å⁻³) along lines joining neighboring Ga-Ga and Ga-Se pairs in various solid and liquid phases.

FIG. 12. Comparison of calculated (open circles) and experimental (filled diamonds) electronic conductivities for liquid $\text{Ga}_{1-x}\text{Se}_x$ alloys.

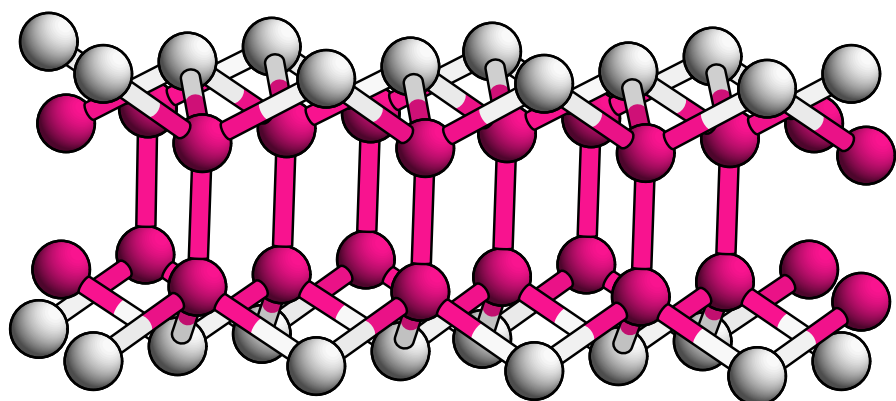
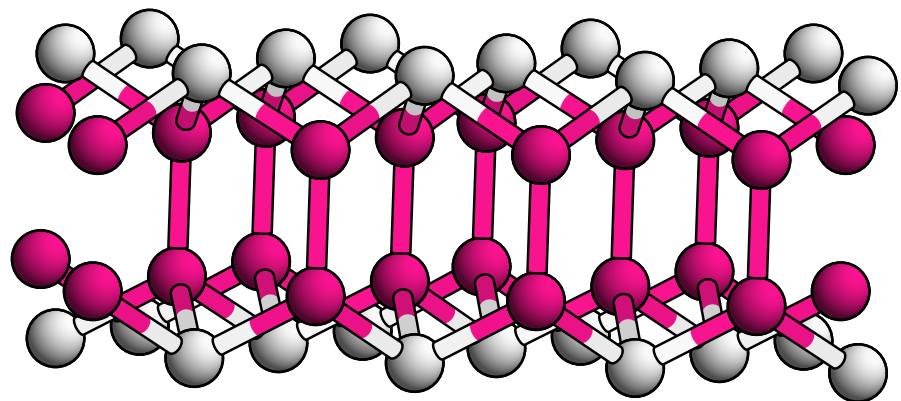
TABLE I. The average coordination numbers for liquid Ga-Se alloys and positions of the first peaks in the radial distribution function, in brackets the interatomic distances and the coordination numbers of the corresponding solid phase. Distances in Å.

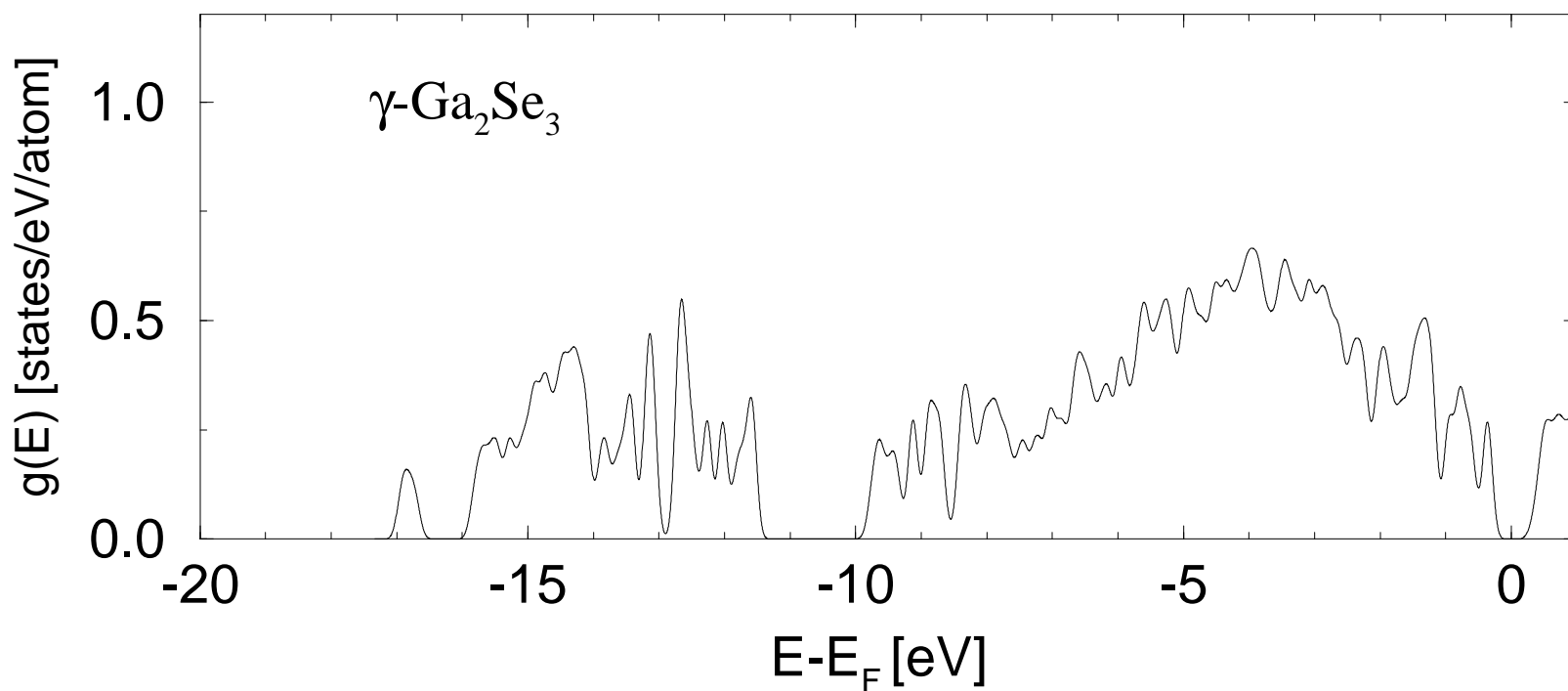
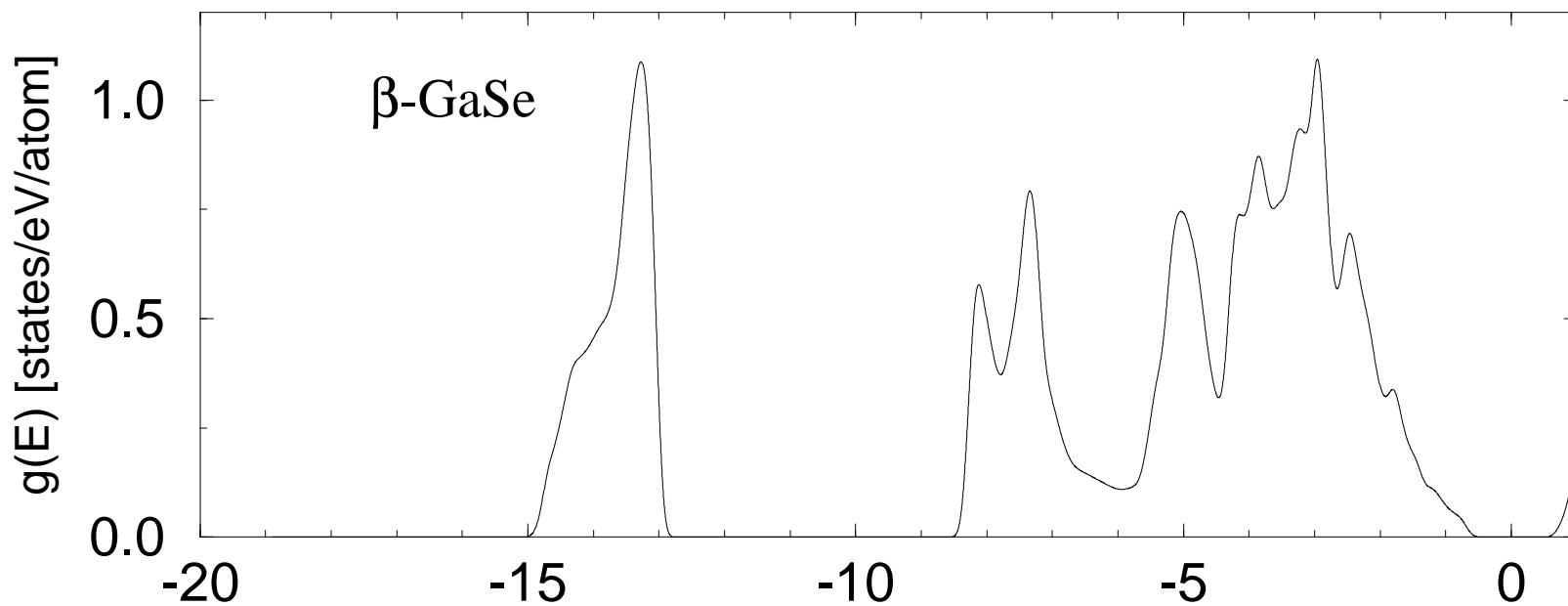
liquid	$r_{\text{Ga-Ga}}$	$n_{\text{Ga-Ga}}$	$r_{\text{Ga-Se}}$	$n_{\text{Ga-Se}}$	$n_{\text{Se-Ga}}$	$r_{\text{Se-Se}}$	$n_{\text{Se-Se}}$
Ga_2Se	2.54	2.41	2.44	1.46	2.92	3.95 ^a	6.2 ^a
GaSe	2.51 (2.44)	1.12 (1)	2.44 (2.45)	2.66 (3)	2.66 (3)	3.95 ^a (4.75 ^a)	8.0 ^a (9 ^a)
Ga_2Se_3	2.46 (3.85 ^a)	0.62 (0)	2.43 (2.35)	3.39 (4)	2.26 (2.67)	3.95 ^a (3.85 ^a)	9.0 ^a (12 ^a)

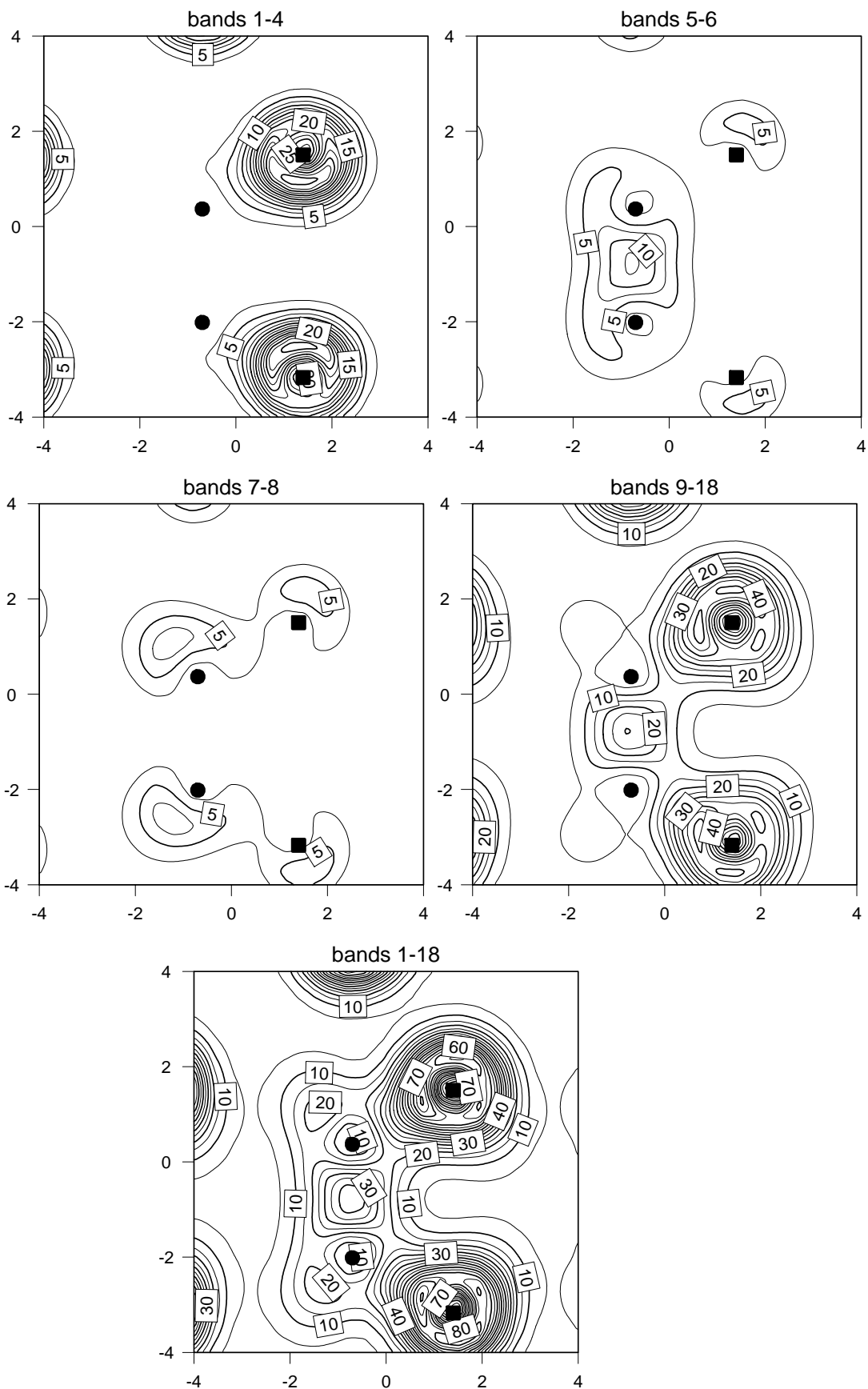
^a these numbers correspond to the second coordination shell.

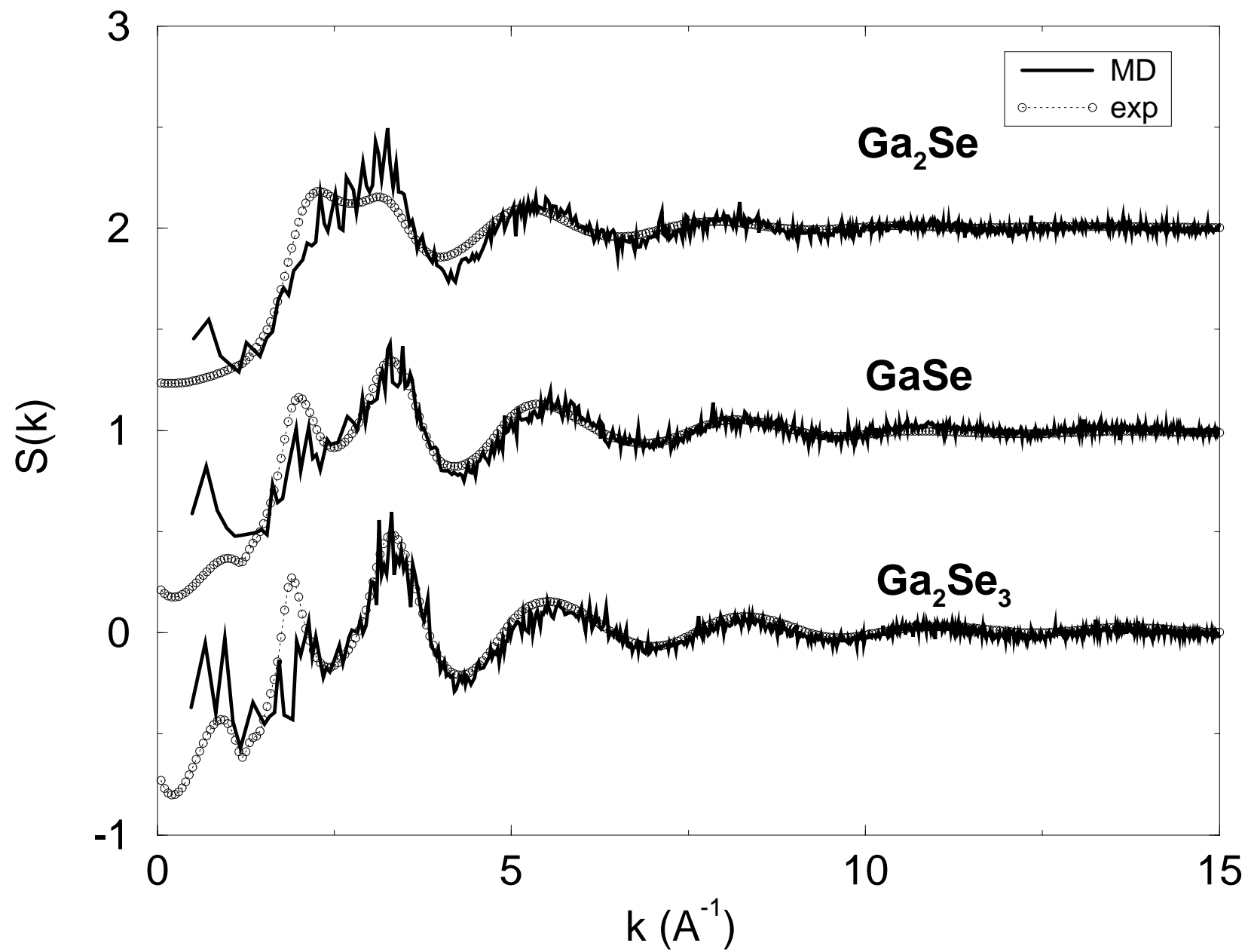
TABLE II. Calculated diffusion coefficients (in $10^{-5}\text{cm}^2\text{s}^{-1}$) for Ga-Se liquids.

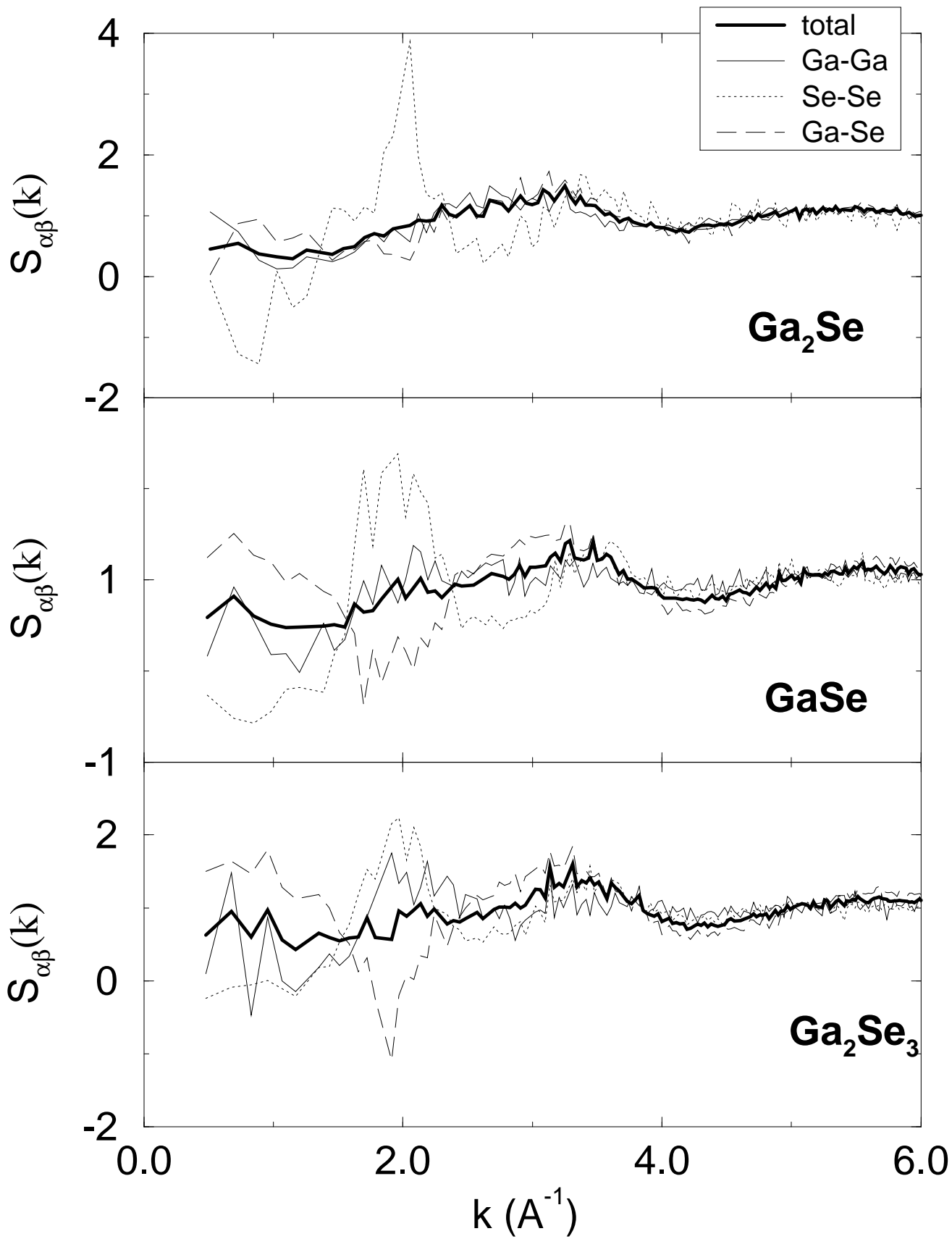
liquid	D_{Ga}	D_{Se}
Ga_2Se	9.8	5.8
GaSe	4.6	3.0
Ga_2Se_3	2.2	2.5

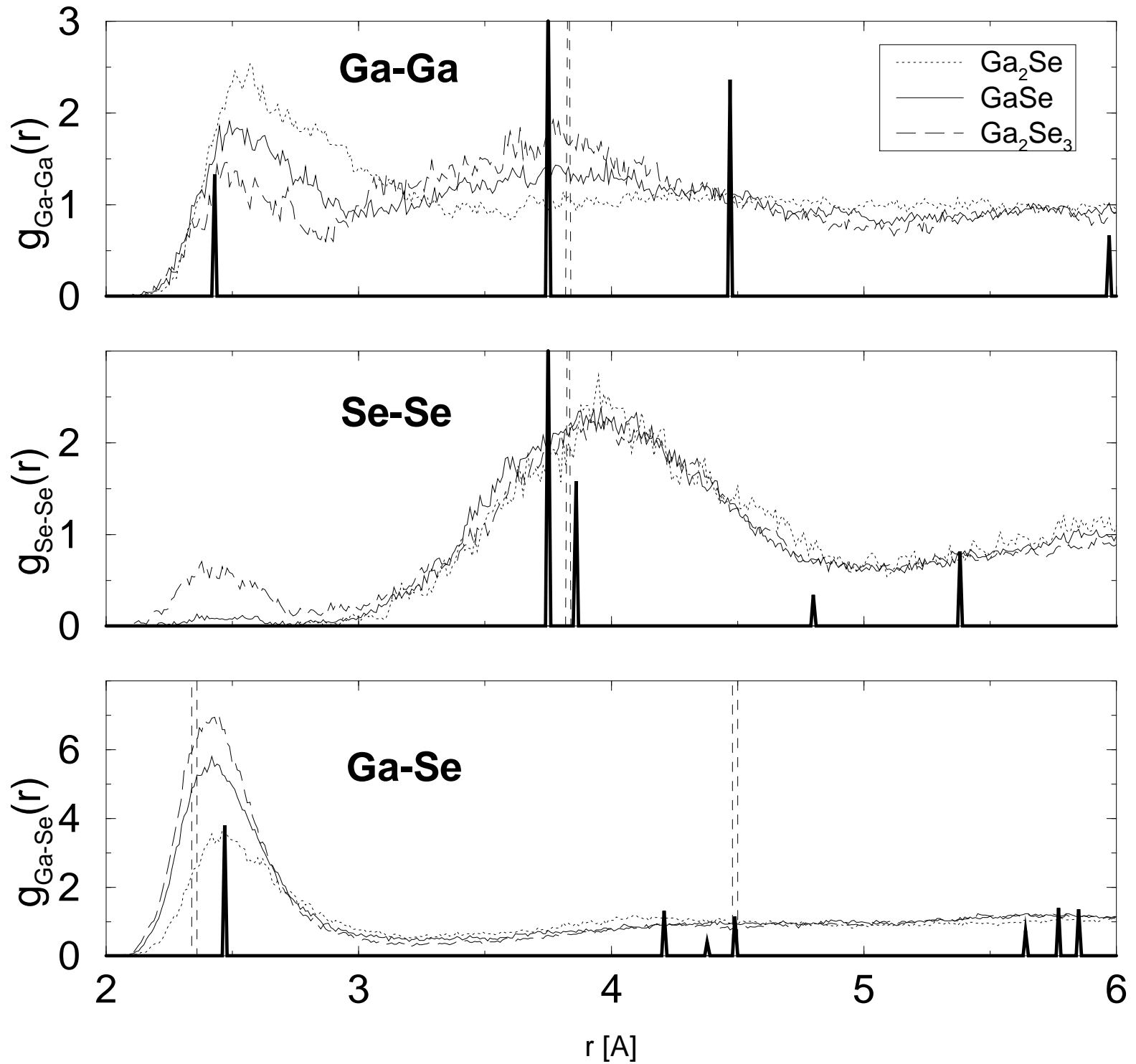


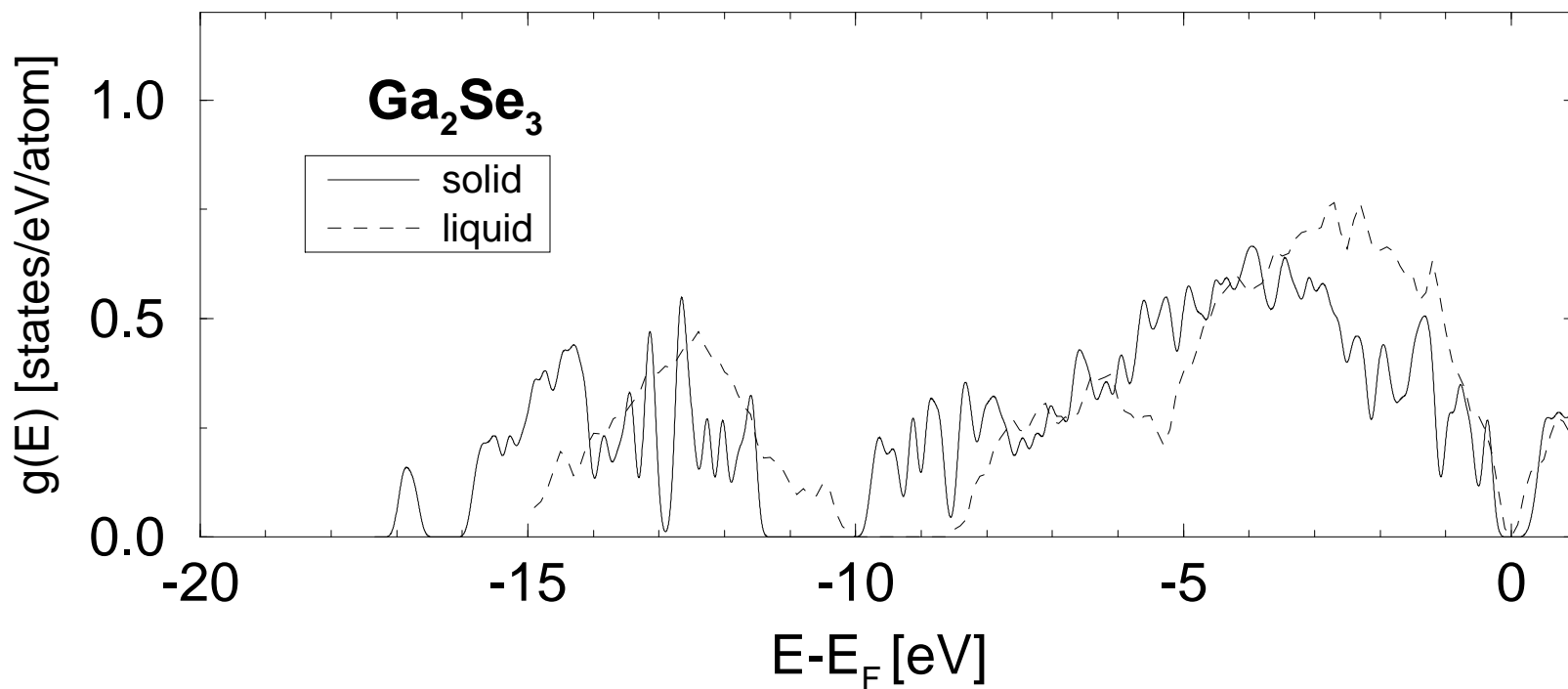
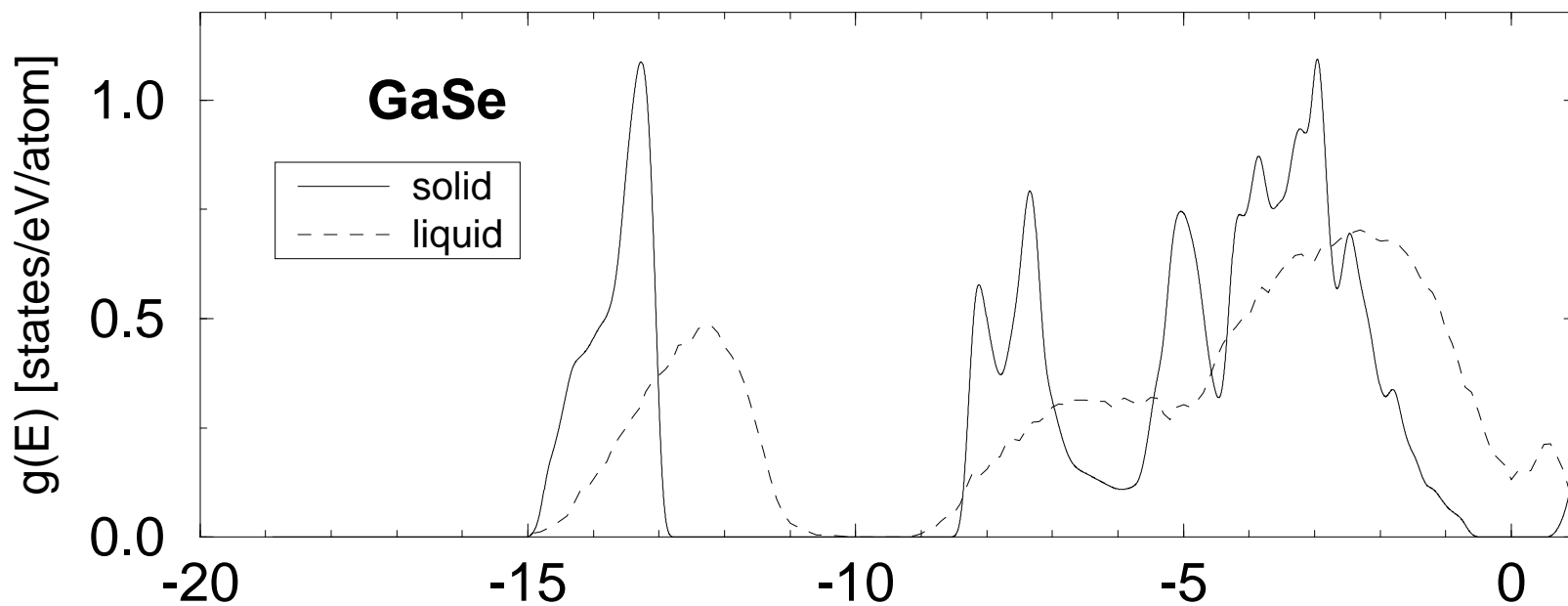


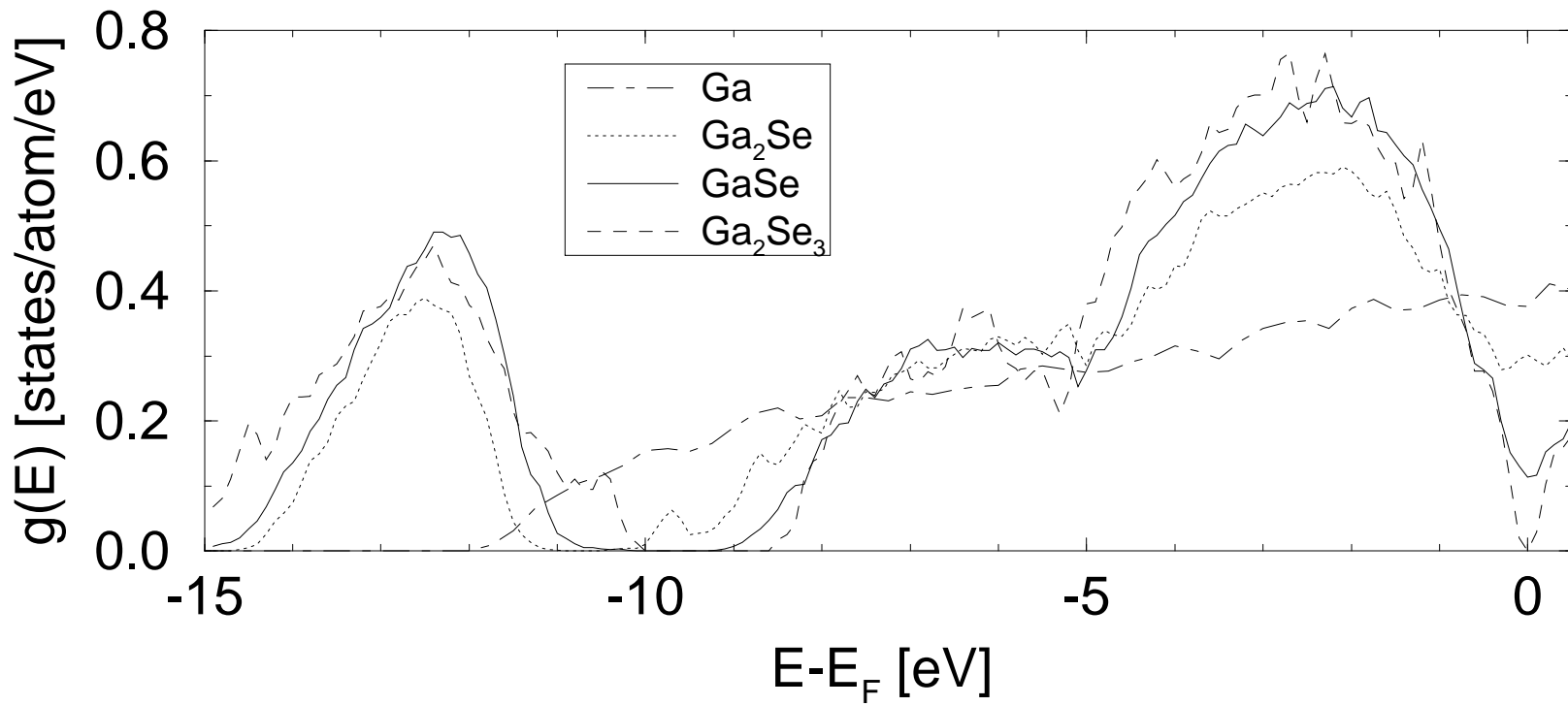


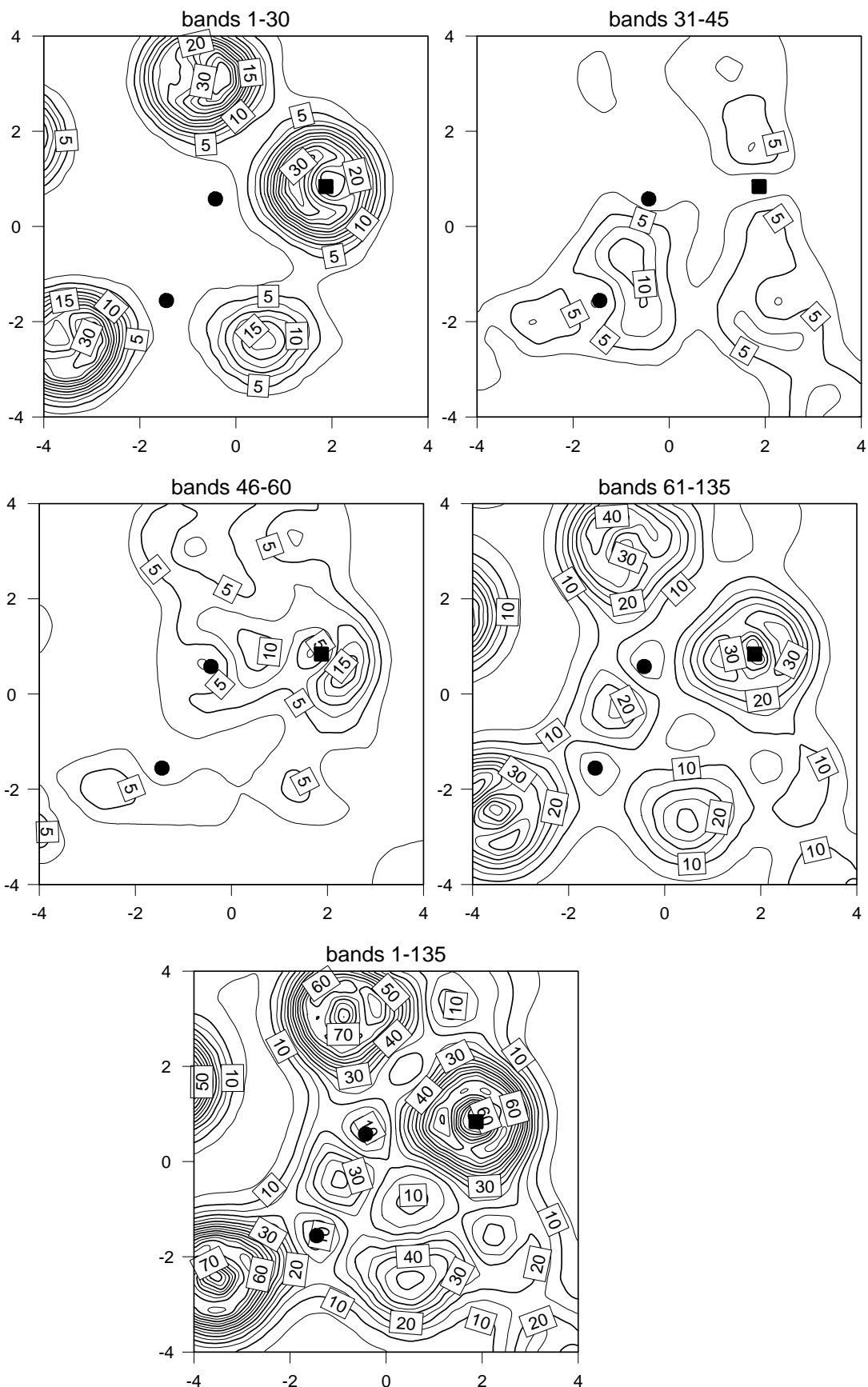


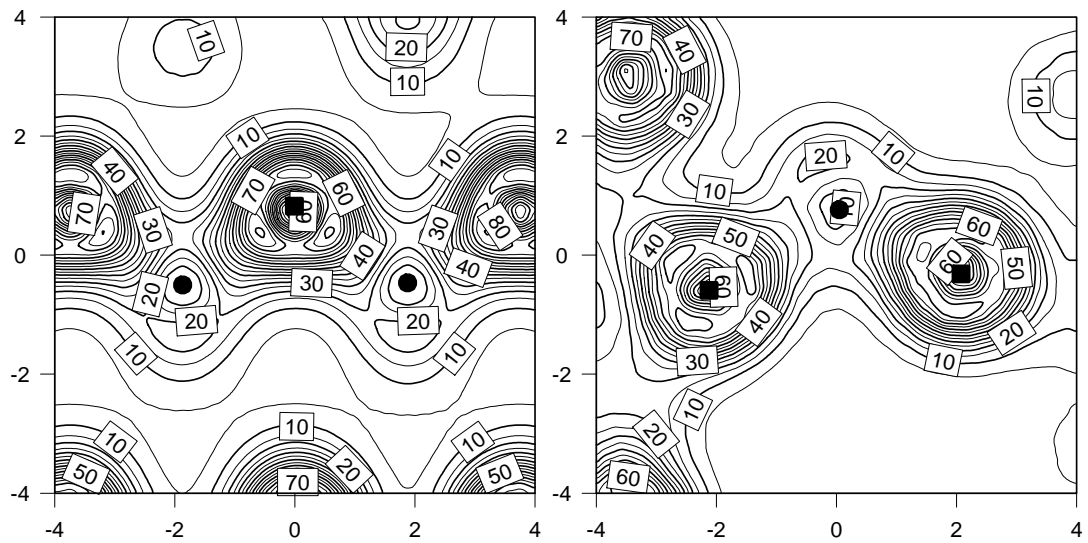


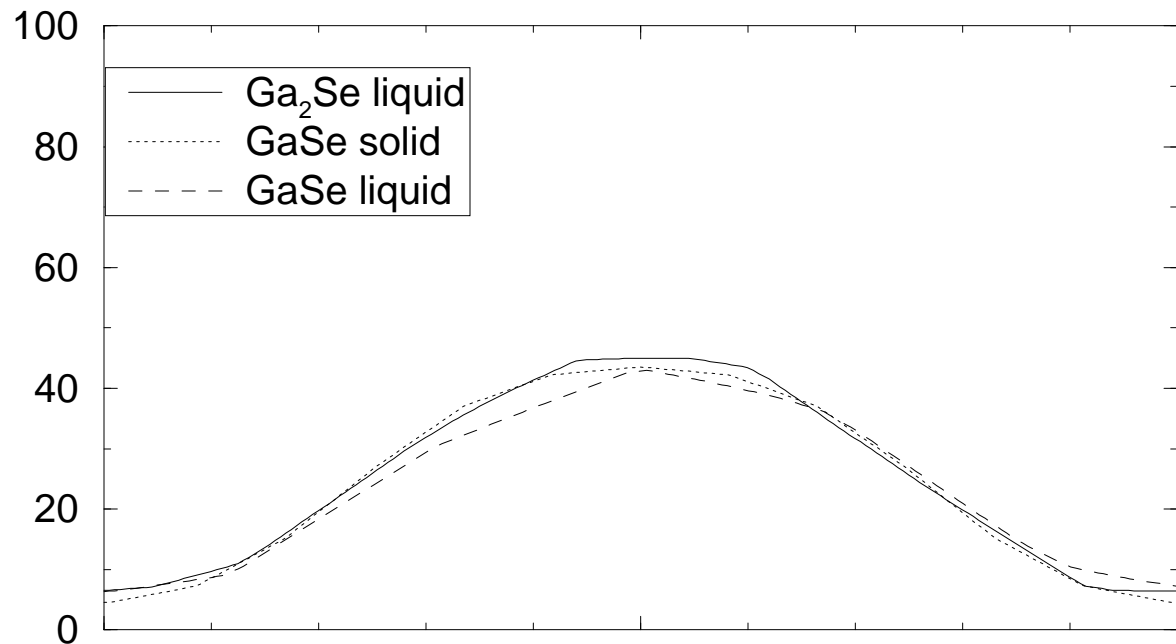






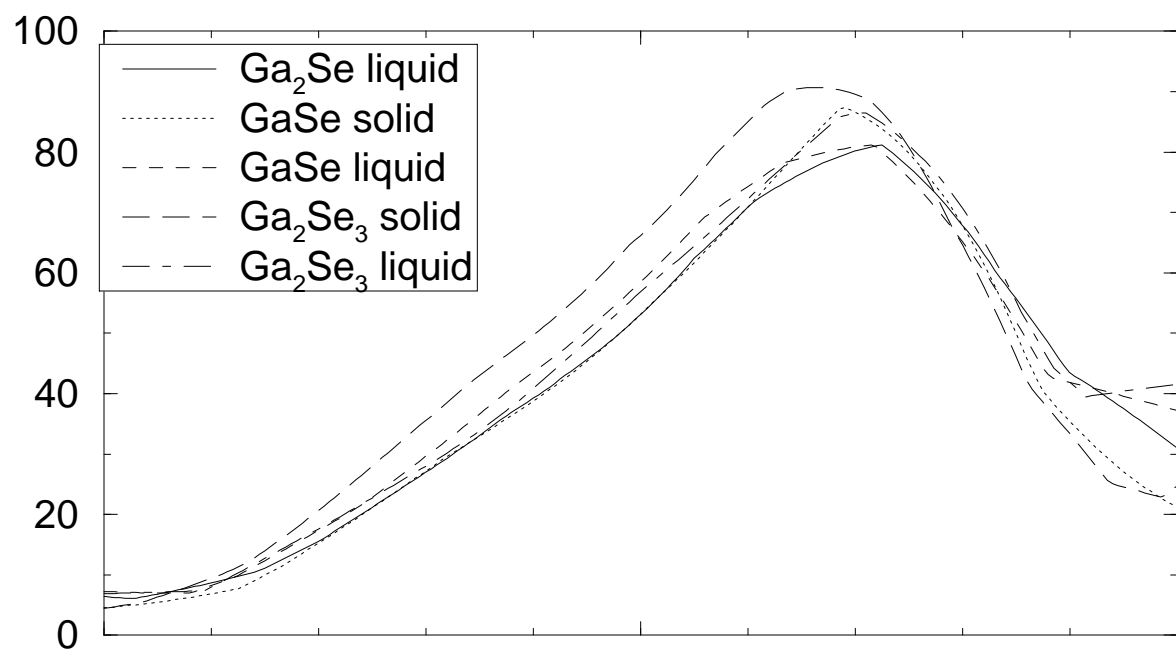






Ga

Ga



Ga

Se

conductivity

